# Two and three dimensional numerical analyses of excavation damaged zones around deep geological repositories in sedimentary rocks

H. Abdi, E. Evgin & M. Fall
*Department of Civil Engineering, University of Ottawa, Ottawa, Ontario, Canada*
T.S. Nguyen & G. Su
*Canadian Nuclear Safety Commission (CNSC), Ottawa, Ontario, Canada*

ABSTRACT
The excavation and operation of potential radioactive waste repositories and the subsequent natural events can result in alterations of the Thermal (T)-Hydrological (H)-Mechanical (M)-Chemical (C) characteristics of the host rock. The excavation of the repository is possibly the main cause of mechanical disturbance, resulting in an excavation damaged zone (EDZ). It is necessary to know the size of the EDZ and the intensity of damage in the rock mass within the EDZ. This investigation shows (a) the differences between the results of two and three dimensional analyses and (b) the effect of the excavation of a second emplacement room on the extent of the EDZ.

RÉSUMÉ
L'excavation et l'opération des ouvrages de stockage des déchets nucléaires, et les événements naturels qui suivent peuvent modifier les caractéristiques thermiques, hydrauliques, mécaniques et chimiques (THMC) de la roche. L'excavation est probablement la cause principale de perturbation mécanique, créant une zone endommagée. Il est nécessaire de connaître la taille et l'intensité de cette zone endommagée. Cette étude montre (a) les différences entre les résultats d'une analyse bi- et tridimensionnelle et (b) l'effet de l'excavation d'une second galerie sur l'étendue de la zone endommagée.

## 1 INTRODUCTION

Deep geological repositories (DGR) are being considered in many parts of the world to contain and isolate radioactive waste. The excavations of a DGR can result in damage in the rock and enhance rock mass permeability. The extent of the excavation damaged zones (EDZ) in the vicinity of the underground openings depends on the in-situ stresses, material properties, and excavation techniques. Field and laboratory studies and numerical analyses have been carried out by many researchers to assess the effect of the EDZ on the thermal, hydrological, mechanical, and chemical characteristics of rock masses (Sato et al. 2000, Souley et al. 1999, Bossart et al. 2004, Tsang et al. 2005, Nguyen 2007, and Kwon and Cho 2008). Underground research laboratories (URL) have been constructed in different countries including Canada, France, Switzerland, Belgium, Japan, Sweden, and South Korea. The types of rock formations encountered in these URL sites include crystalline rocks, rock salt, and argillaceous rocks.

Ontario Power Generation (OPG) is planning to develop a deep geologic repository in southern Ontario to host low-level and intermediate-level (LILW) nuclear wastes resulting from the operation of its CANDU reactors. The location for the repository is within an Ordovician limestone.

The objectives of the present work are as follows: (1) to assess the extent of damage caused by the excavation of emplacement rooms, (2) to determine the differences in the results of 2D and 3D analyses with respect to stresses and deformations in the rock mass around a DGR, and (3) to evaluate the effect of the excavation of a second emplacement room on the extent of EDZ.

## 2 GEOLOGY AT THE DGR SITE

Figure 1 shows the rock formations at the site of the proposed DGR for LILW. The types of rock include carbonates, shale, evaporate and sandstone. The repository would be located at an approximate depth of 683 m in the Cobourg limestone with low permeability (lower than $10^{-21}$ $m^2$). The groundwater at the repository level has a relatively high concentration of dissolved solids, and is saline. In-situ horizontal stresses at the proposed site are higher than the vertical stress. According to the regional data (OPG Report -1, 2008), the maximum in-situ horizontal stress is around 2 times the in-situ vertical stress. The minimum in-situ horizontal stress is about 1.1 times the in-situ vertical stress. In the analysis, it is conservatively assumed that the maximum in-situ horizontal stress is acting perpendicular to the axes of the emplacement rooms and the direction of the minimum in-situ horizontal stress is parallel to the axes of the emplacement rooms. In the present analyses, all emplacement rooms are excavated at the same elevation at a depth of 683 m below the ground surface. The emplacement rooms are of rectangular shape (7.5 m height x 8.1 m width), and the horizontal distance between the two adjacent emplacement rooms is 16 m.

## 3 FINITE ELEMENT MODELS

Four rock layers around the emplacement rooms are included in the numerical analysis. These four layers (from the bottom-up) are: Sherman Fall (layer 1), Weak Sherman Fall (layer 2), Cobourg (layer 3), and Shale (layer 4) as shown in Figure 2. The dimensions of the analysis domain are 120 m along the x-axis (horizontal) and 103 m along the y-axis (vertical) for 2D analysis. In the 3D analysis, the dimensions of the analysis domain are 120 m along the x-axis (horizontal), 40 m along the y-axis (horizontal), and 103 m along the z-axis (vertical).

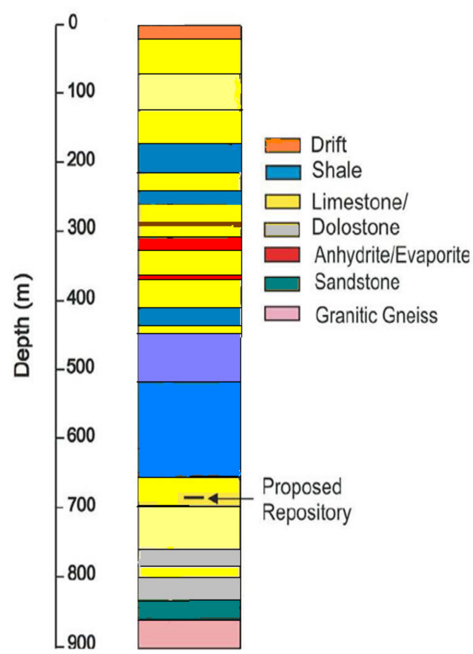


Figure 1. Rock formations (modified from Jensen et al. 2009)

The boundary conditions are as follows. The vertical boundaries are fixed horizontally, which means only vertical movements of the material are allowed at these boundaries. The top boundary is subjected to a uniform vertical load equivalent to the in-situ vertical stress. The base of the model is fixed. Plane strain conditions are imposed in 2D analysis.

### 3.1 Constitutive Relation and Parameters

Field and laboratory measurements of the geotechnical properties of the rock layers are obtained from open literature. The Drucker-Prager constitutive relation is used for all rock formations. For each rock layer, the average values of the elastic modulus, Poisson's ratio, unit weight, cohesion, and friction angle are required in the analysis. Table 1 summarizes the data used for these four layers (OPG Report - 2, 2008).

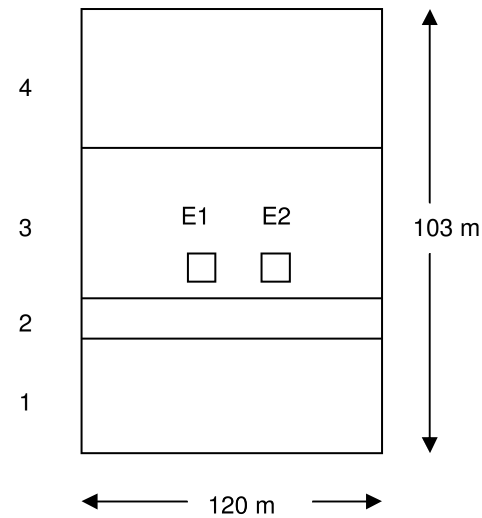


1 = Sherman Fall (30 m high)
2 = Weak Sherman Fall (10 m high)
3 = Cobourg (33 m high)
4 = Shale (30 m high)
E1 = Emplacement room-1
E2 = Emplacement room-2

Figure 2. Model geometry

Table 1. Geotechnical data (From OPG Report - 2, 2008)

| Type of rock | E (GPa) | *v* | C (MPa) | Φ, deg |
|---|---|---|---|---|
| *Sherman Fall* | *26.45* | *0.23* | *12.4* | *45* |
| *Weak Sherman* | *10.74* | *0.08* | *6.23* | *45* |
| *Cobourg* | *36.04* | *0.19* | *19.09* | *45* |
| *Shale* | *7.3* | *0.09* | *6.46* | *45* |

## 4 RESULTS OF NUMERICAL ANALYSES

The numerical results are described in two sections. The first section consists of 2D results and the second section consists of 3D results. In this paper, only the data related to the various stress distributions, effective plastic strains, volumetric strains, shear strains, and displacements at the crown, the invert, and the springlines are presented. The sign convention for normal stresses plotted in the figures is as follows: a negative stress means compression and a positive stress means tension.

4.1 Two Dimensional Analyses

Two types of 2D analysis are carried out. In the first analysis, only one room is excavated (E1 in Fig. 2). The excavation process is simulated by gradually reducing the geotechnical properties of the excavated region, initial stresses, and body load from initial values to negligible values. In the second type of analysis, two rooms are excavated. The second room (E2 in Fig. 2) is excavated after completing the excavation of the first room (E1). The simulation of the excavation process for the second room followed the same procedure as the one used for the first room.

- Excavation of one emplacement room

Stress distributions

Figure 3 shows the distribution of the vertical compressive stress after the excavation. Contour lines of the compressive stress with a magnitude less than 2e7 Pa are not plotted to maintain clarity. Before the excavation, the magnitude of the vertical compressive stress acting at the level of excavation was about 1.8e7 Pa. The vertical compressive stress acting on a horizontal surface extending from the right-bottom corner to the right boundary is plotted in Fig. 4. The horizontal line shown in this figure is the value of the vertical stress before the excavation. The magnitude of the maximum vertical compressive stress along this line is 3.4e7 Pa and it occurred at the corner of the emplacement room.

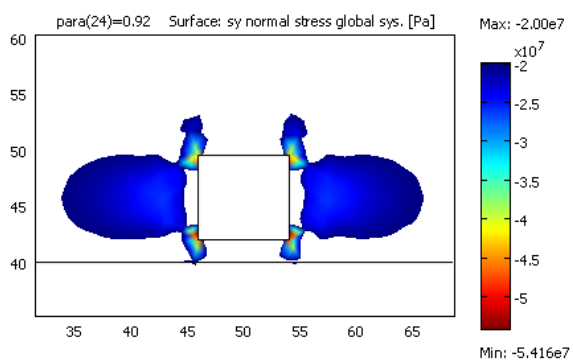


Figure 3. Distribution of vertical compressive stress after the excavation of the first room.

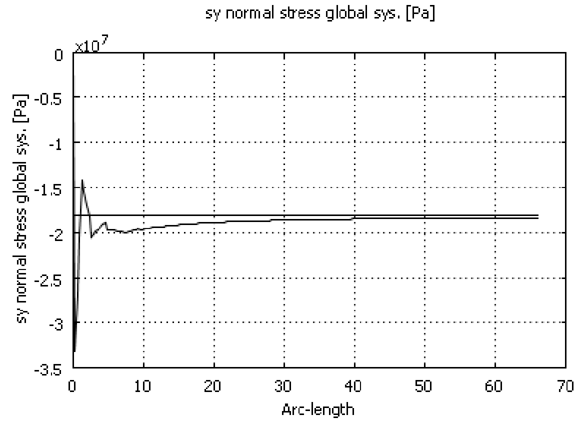


Figure 4. Variation of the vertical stress acting along a line between the right-bottom corner and the right boundary.

Figure 5 shows the distribution of the horizontal compressive stress at the end of the excavation. Before the excavation, the magnitude of the horizontal compressive stress acting at the level of excavation was about 3.6e7 Pa. The magnitude of the maximum horizontal compressive stress in the whole analysis domain is 8.45e7 Pa and it occurs at the corners of the emplacement room. Figure 6 shows an example of the variation of the horizontal stress at points along the line between the right-top corner and the top boundary. The nearly horizontal line shown in this figure represents the distribution of the horizontal compressive stress before the excavation. The magnitude of the maximum horizontal compressive stress is 6e7 Pa along this line.

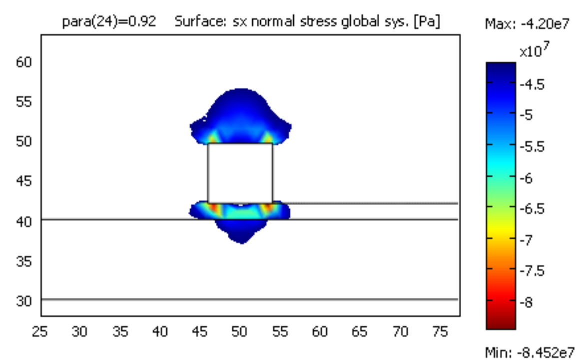


Figure 5. Distribution of horizontal compressive stress after the excavation of the first room.

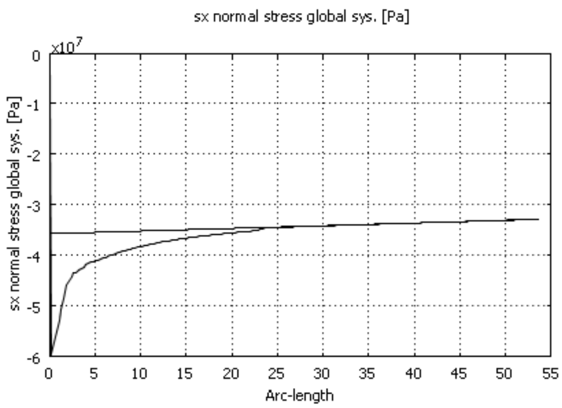


Figure 6. Variation of the horizontal stress acting along a line between the right-top corner and the top boundary.

Effective plastic strains

Figure 7 shows the effective plastic strains, >0.0001, developed as a result of excavation. Plastic strains are developed at the corners of the room and within the weak Sherman Fall layer located at 2 m beneath the room. The calculated maximum value of plastic strain is 0.0022. The effective plastic strain (EPS) can be used as a measure of damage in the rock mass. Nguyen (2007) used EPS to predict changes in the permeability in the excavation damaged zone around a tunnel.

Volumetric strains

Figure 8 shows the distribution of volumetric strains larger than 0.0001. Large expansive volumetric strains are

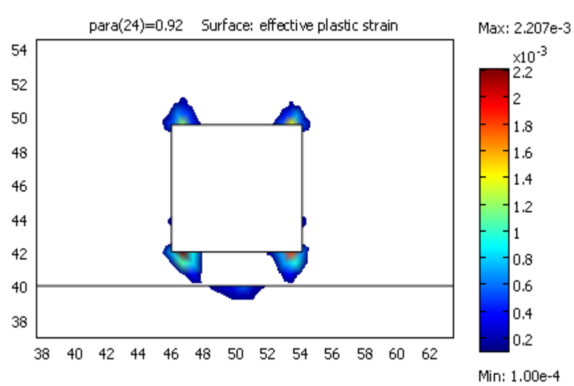


Figure 7. Distribution of effective plastic strains, >0.0001, after the excavation of the first room.

developed on the right and left sides of the room. Volumetric strains are also developed above and below the room and within the weak Sherman Fall layer located at 2 m beneath the room. These results show that some expansion of the rock mass will occur and possibly the permeability of the material will increase as a result of the excavation.

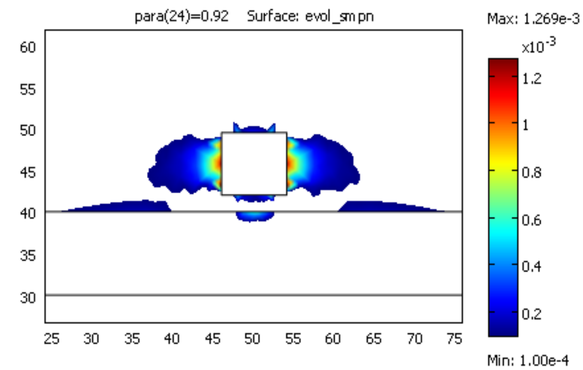


Figure 8. Distribution of volumetric strains, > 0.0001, after the excavation of the first room.

- Excavation of two emplacement rooms

Stress distributions

In the calculations, the second emplacement room is excavated after completing the excavation of the first room. Figure 9 shows the distribution of the vertical compressive stress after the excavation. The magnitude of the maximum compressive stress is 6.4e7 Pa and it occurred at the corners. Before the excavation, the magnitude of the vertical stress acting at the level of excavation was about 1.8e7 Pa. The vertical stress acting on a horizontal surface between the rooms is plotted in Fig. 10. The horizontal line shown in this figure is the magnitude of the vertical compressive stress before the excavation. The magnitude of the maximum compressive stress along this particular line is about 2.8e7 Pa and it occurred at a distance about 3 m away from the walls of the rooms.

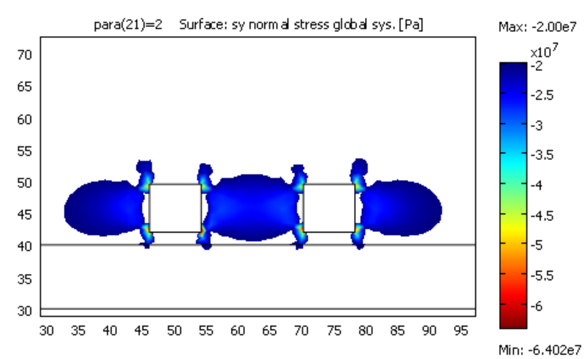


Figure 9. Distribution of vertical normal stress after the excavation of two rooms

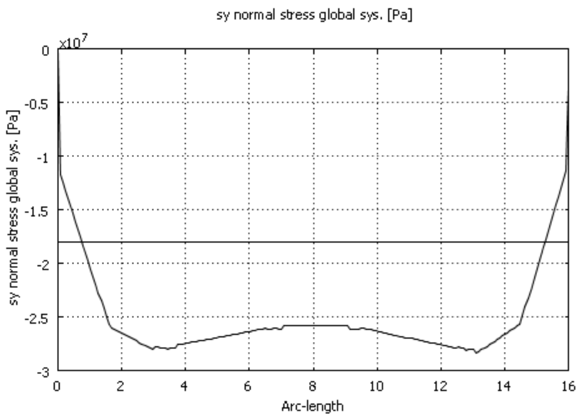


Figure 10. Variation of $\sigma_y$ between the two rooms (at the level of springlines)

Figure 11 shows the distribution of the horizontal compressive stress at the end of the excavation. Before the excavation, the magnitude of the horizontal compressive stress acting at the level of excavation was about 3.6e7 Pa. After the excavation, the magnitude of the maximum horizontal stress is 8.16e7 Pa and it occurs at the corners of the rooms.

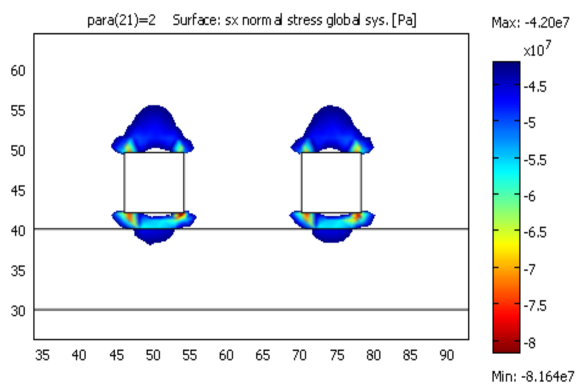


Figure 11. Distribution of horizontal compressive stress after the excavation of two rooms.

Effective plastic strains

Figure 12 shows the distribution of the effective plastic strains, >0.0001, after the excavation. Areas of plastic strains are developed at the corners of the rooms and within the weak Sherman Fall layer located at a distance of 2 m underneath the rooms.

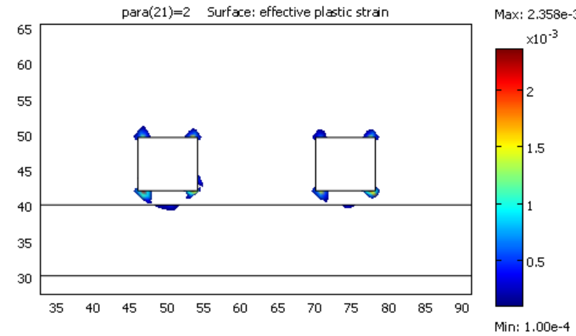


Figure 12. Distribution of plastic strains, >0.0001, after the excavation of two rooms.

Volumetric strains

Figure 13 shows the distribution of volumetric strains, >0.0001. Large volumetric strains are developed on the right and left sidewalls, below and above the rooms, and within the weak Sherman Fall layer located at 2 m below the rooms.

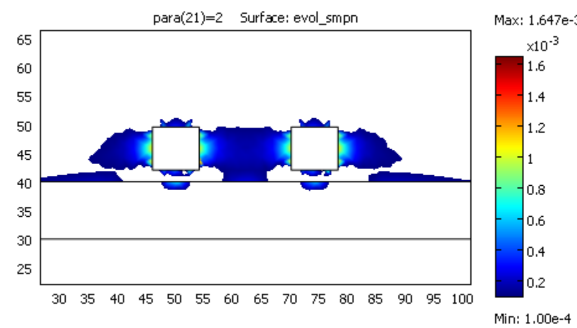


Figure 13. Distribution of volumetric strains, >0.0001, after the excavation of two rooms.

Shear stresses

Figure 14 shows contours of shear stresses which are developed as a result of excavation. The top-left and bottom-right corners of the rooms are subjected to negative shear stresses, while the remaining corners are subjected to shear stresses with positive sign.

4.2 Three Dimensional Analyses

3D simulations are also carried out for the excavation of one and two emplacement rooms. In the first case, only one room is excavated (Room E1 in Fig. 2). As in 2D analysis, the room has a rectangular cross section (8.1 m in the x-direction and 7.5 m in the z-direction) and has a length of 10 m (in the y-direction). The excavation process is simulated by dividing the room into 10 slices. The simulation of the excavation is carried out by gradually reducing the values of the parameters of

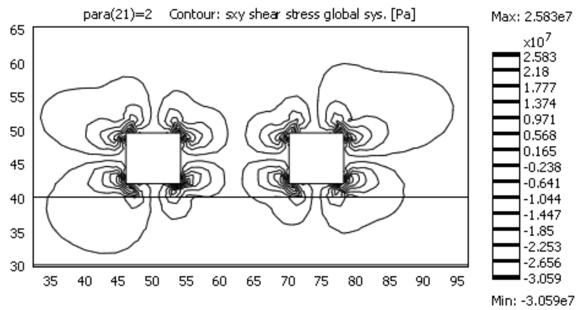


Figure 14. 2D contours of shear stresses after the excavation of two rooms.

geotechnical properties, initial stresses, and body load from initial values to negligible values. In order to simulate the construction stages, the first slice is excavated starting at the room face. This process is repeated sequentially for all slices until the tenth slice. Similar to the 2D analyses, two types of simulations are carried out. In the first type of analysis, only one room is excavated (E1 in Fig. 2). In the second type of analysis, two rooms are excavated one after the other but not simultaneously. The second room (E2 in Fig. 2) is excavated after completing the excavation of the first room (E1). The horizontal distance between the two rooms is 16 m. The simulation of the excavation process for the second room followed the same procedure as the one used for the first room.

- Excavation of one emplacement room

Stress distributions

Stress states in the rock around the emplacement rooms change each time when a slice of the rock mass is removed from the analysis domain. Figure 15 shows the distribution of the vertical compressive stress after the excavation of the emplacement room E1.

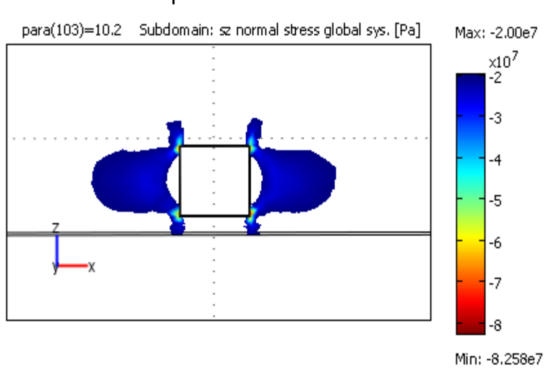


Figure 15. Distribution of vertical compressive stress after the excavation.

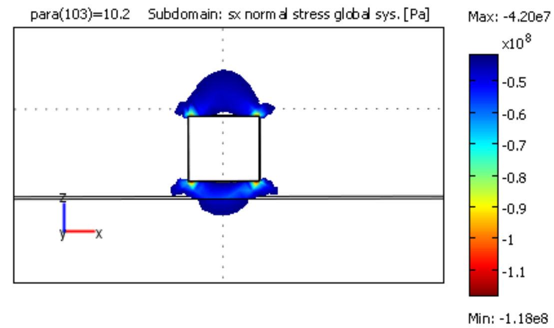


Figure 16. Distribution of $\sigma_x$ after the excavation.

Figure 16 shows the distribution of the horizontal compressive stress after the excavation. High stresses shown in Figures 15 and 16 start to develop at the room face and the magnitude of stresses depends on the excavation stages. The maximum vertical compressive stress (8.25e7 Pa) and the maximum horizontal compressive stress (11.8e7 Pa) are developed at the corners of the room.

Effective plastic strains

Figure 17 shows the effective plastic strains, >0.00004, developed after the excavation. Plastic strains are developed at the corners of the room. The highest value of plastic strains is around 0.001.

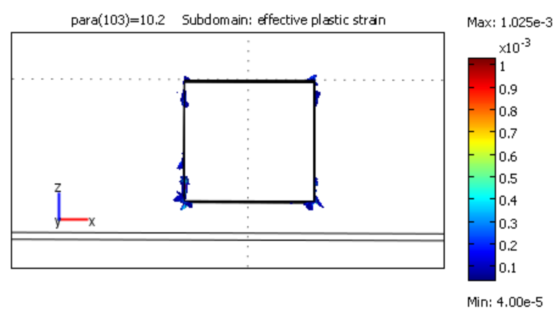


Figure 17. Distribution of effective plastic strains, >0.00004.

Volumetric strains

Figure 18 shows the distribution of expansive volumetric strains, > 0.0001, after the excavation. Largest volumetric strains are developed on the right and left sides of the room, underneath and above the room, and also within the weak Sherman Fall layer.

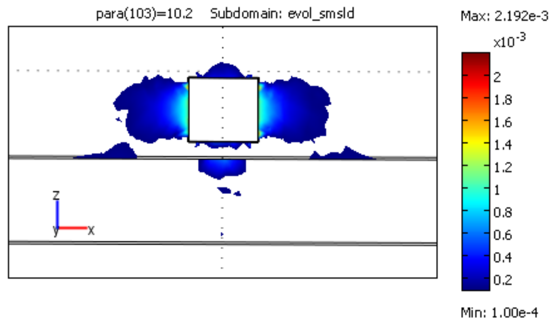


Figure 18. Distribution of volumetric strains, >0.0001,

- Excavation of two emplacement rooms

Stress distributions

The second room is excavated after completing the excavation of the first room. Figures 19 and 20 show the distribution of vertical and horizontal stresses after the excavation. High stresses develop around the first emplacement room where the excavation starts first. As the excavation advances in the horizontal direction, the intensity of the stresses change and the size of the highly stressed areas of rock become larger along the emplacement room. The excavation of the second room has no significant additional effect in terms of the development of high stresses.

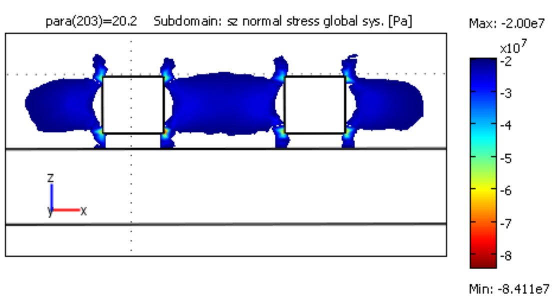


Figure 19. Distribution of $\sigma_z$ after excavating two rooms.

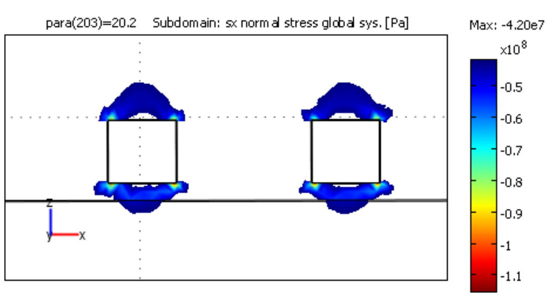


Figure 20. Distribution of $\sigma_x$ after excavating two rooms.

Effective plastic strains

Figure 21 shows the distribution of effective plastic strains, >0.00004. Plastic strains are larger at the corners of the rooms. The size of the regions of large plastic strains depends on the excavation stages. The maximum value of the effective plastic strain is around 0.002.

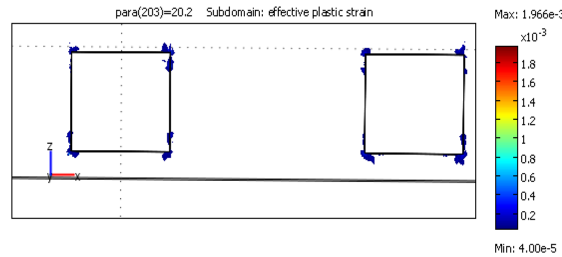


Figure 21. Distribution of effective plastic strains, >0.00004, after excavating two rooms.

Volumetric strains

The distribution of expansive volumetric strains, >0.0001, is shown in Figure 22. Large volumetric strains are developed on the right and left sides of the rooms, underneath and above the rooms, and also within the weak Sherman Fall layer. Figure 23 shows the magnitude of the volumetric strains between the springlines of two rooms.

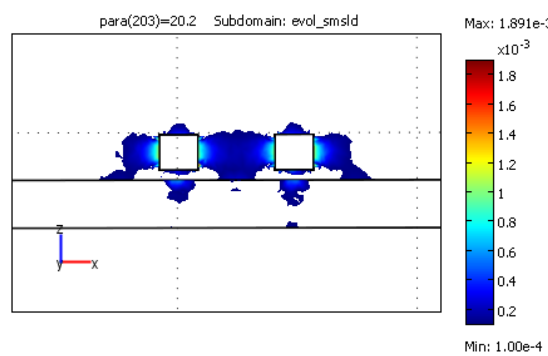


Figure 22. Distribution of volumetric strains, >0.0001.

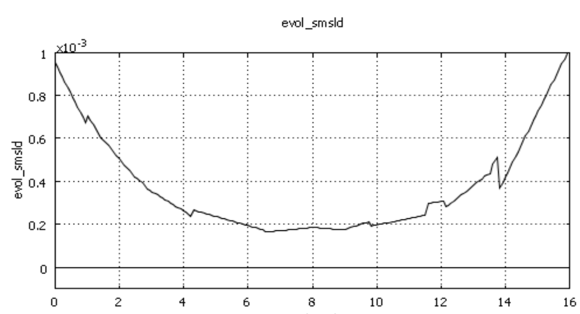


Figure 23. Variation of volumetric strains between the two rooms (spring line).

Shear strains

Table 2 lists the values of shear strains, obtained from 2D and 3D analyses, at the corners of the rooms. Negative shear strains are calculated for the top-left and bottom-right corners of the rooms. Whereas, positive shear strains are calculated for the top-right and bottom-left corners of the rooms. The excavation of the second room causes development of slightly more shear strains.

Table 2: 2D and 3D shear strains at the top-left-corner (TLC), top-right-corner (TRC), bottom-left-corner (BLC), and bottom-right-corner (BRC) of the rooms.

| Shear Strain, x10$^{-3}$ | TLC | TRC | BLC | BRC |
|---|---|---|---|---|
| 2D Analysis (one room) | -2.2 | 2.2 | 2.6 | -2.6 |
| 3D Analysis (one room) | -2.6 | 2.6 | 2.8 | -2.8 |
| 2D Analysis (two rooms) | | | | |
| Room 1 | -2.2 | 2.1 | 2.6 | -2.8 |
| Room 2 | -2.0 | 2.3 | 2.5 | -2.7 |
| 3D Analysis (two rooms) | | | | |
| Room 1 | -2.5 | 2.5 | 2.7 | -3.2 |
| Room 2 | -2.5 | 2.5 | 2.7 | -3.1 |

Table 3 gives the displacements calculated at the crown, the invert, and springlines of one and two rooms. The numbers correspond to both the 2D and 3D analyses of the displacements at the face of the rooms. According to 2D analysis, inward displacements of about 6.3, 9.4, and 9.2 mm are generated on the floor and the left and right sides of the rooms, respectively. The downward displacement at the crown is around 4 mm. The excavation of the second room cause more

Table 3: 2D and 3D displacements (mm) at the crown (YDC), the invert (YDI), left springline (XDLS), and right springline (XDRS) for one and two rooms.

| *Displacement (mm)* | *YDC* | *YDI* | *XDLS* | *XDRS* |
|---|---|---|---|---|
| *2D Analysis (one room)* | *3* | *6.3* | *8.5* | *8.5* |
| *3D Analysis (one room)* | *2.8* | *6.2* | *7.5* | *7.5* |
| *2D Analysis (two rooms)* | | | | |
| *Room 1* | *4.3* | *6.2* | *9.4* | *5.5* |
| *Room 2* | *4.3* | *6.2* | *5.5* | *9.2* |
| *3D Analysis (two rooms)* | | | | |
| *Room 1* | *3.2* | *6.4* | *7.8* | *5.7* |
| *Room 2* | *3.2* | *6.4* | *5.7* | *7.8* |

Table 4: Inward displacements (mm) of rock mass along the length of emplacement rooms.

| y-distance | *0 m* | *4m* | *6 m* | *8 m* | *10 m* |
|---|---|---|---|---|---|
| One Emplacement Room | | | | | |
| Crown | *2.8* | *2.7* | *2.6* | *2.2* | *0.3* |
| Invert | *6.2* | *6* | *5.9* | *4.1* | *1.1* |
| Springline (left) | *7.5* | *7.1* | *6.6* | *5.5* | *1.8* |
| Springline (right) | *7.5* | *7.2* | *6.7* | *5.6* | *2* |
| Two Emplacement Rooms | | | | | |
| Room 1 | | | | | |
| Crown | *3.2* | *3.2* | *2.8* | *2.5* | *0.6* |
| Invert | *6.4* | *6.2* | *5.5* | *4.2* | *1* |
| Springline (left) | *7.8* | *7.5* | *7* | *6* | *2.1* |
| Springline (right) | *5.7* | *5.5* | *5.2* | *4.4* | *1.1* |
| Room 2 | | | | | |
| Crown | *3.2* | *3.1* | *2.9* | *2.4* | *0.6* |
| Invert | *6.4* | *6* | *5.5* | *4.1* | *1.1* |
| Springline (left) | *5.7* | *5.6* | *5.3* | *4.5* | *1.1* |
| Springline (right) | *7.8* | *7.5* | *7* | *5.8* | *2.3* |

displacements in the roofs of both rooms (up to 40%), less displacement on the right-side of the first room (-30%), and less displacement on the left-side of the second room (-30%). 2D analysis predicts up to 30% more displacements than the 3D analysis.

According to the data of 3D analysis reported in Table 4, most of the deformation produced by excavation at any point in the emplacement room takes place by the time the excavation moves 4 meters away from this point.

## 5 CONCLUSIONS

The conclusions of this numerical study are as follows:

- Due to the excavation, high vertical and horizontal stresses are developed at the corners and close to the walls of the rooms. The amount of increase in the vertical stress is up to 300% as compared to the far field stresses. Similarly, the increase in the horizontal stress is up to 200%. The highest stresses are calculated at the corners of the rooms for both 2D and 3D analyses.
- Large volumetric strains, effective plastic strains, and shear strains are developed around the rooms, in between the rooms and within the weak Sherman Fall layer. In these areas of high strains, the rock mass is expected to experience damage. In the excavation damaged zones, it is likely to see a reduction in the strength of rock mass, increase in crack population, expansion of the existing fractures,

and increase in the hydraulic conductivity of the material.

- For 3D analysis, most of the deformation produced by excavation at any point in the emplacement room takes place by the time the excavation moves 4 meters away from this point.
- The size of the EDZ can be approximated as follows: about 5 m on the left side, right side, and below the rooms, and 3 m above the roof of the rooms.
- The excavation of the second room increases the size of the EDZ above the rooms.
- Areas of volumetric strains and plastic strains are developed in the Weak Sherman Fall layer located at 2 m below the base of the emplacement rooms.
- In general, 2D analysis predicts slightly higher values of displacements and effective plastic strains than 3D analysis. On the other hand, 3D analysis predicts slightly higher values of stresses and volumetric strains than 2D analysis.

REFERENCES


Bossart P., Trick T., Meier P.M., Mayor J-C 2004. Structural and hydrogeological characterisation of the excavation-disturbed zone in the Opalinus Clay (Mont Terri Project, Switzerland). Applied Clay Science, 26 (1-4), pp. 429-448.

Jensen M., Lam T., Luhowy D., McLay J., Semec B., and Frizzell R. 2009. Ontario Power Generation's proposed L&ILW deep geologic repository: An overview of geoscientific studies. GeoHalifax 2009. CGS-IAH(CNC), Halifax, NS, Canada.

Kwon S. and Cho W. J. (2008). The influence of an excavation damaged zone on the thermal-mechanical and hydro-mechanical behaviors of an underground excavation. Engineering Geology, 101 (3-4), pp. 110-123.

Nguyen, T. S. 2007. Excavation damage and pore pressure evolutions around a test tunnel in granite, Proceedings of the 2007 Canadian Geotechnical Conference, Ottawa.

OPG Report – 1, 2008. Phase 1 Geosynthesis, Prepared by Gartner Lee Limited, OPG 00216-REP-01300-00010-R00.

OPG Report - 2, 2008. Phase 1 Long-Term Cavern Stability, Prepared by ITASCA Consulting Group, Inc., OPG 00216-REP-01300-00005-R00.

Sato T., Kikuchi T., and Sugihara K. (2000). In-situ experiments on an excavation disturbed zone induced by mechanical excavation in Neogene sedimentary rock at Tono mine, central Japan. Engineering Geology, 56 (1-2), pp. 97-108.

Souley M., Homand F., and Chibout M. 1999. A 3D numerical modeling of damage extension around an underground excavation: Effect of cut-off keys in bulkheadesign. The 37th U.S. Symposium on Rock Mechanics (USRMS), June 7 - 9, Vail, CO.

Tsang C-F, Bernier F., and Davies C. 2005. Geohydromechanical processes in the Excavation Damaged Zone in crystalline rock, rock salt, and indurated and plastic clays—in the context of radioactive waste disposal. International Journal of Rock Mechanics and Mining Sciences, 42 (1), pp. 109-125.